BAND GAP TUNING

Energy states of electrons in a semiconductor consist of bands of energies that are completely occupied (valence bands) followed by unoccupied bands (conduction bands), separated by a gap of forbidden states. The band-gap energy, which is the minimum energy required to promote electrons from the top of the filled valence band to the bottom of the empty conduction band, plays a fundamental role in the optical and electrical properties of a semiconductor. The operating parameters of devices such as lasers, photon detectors, and transistors are determined by this property. Energies of a given band also exhibit dispersion, i.e., dependence on the crystal momentum vector. The direct band-gap semiconductors (e.g., gallium arsenide, or GaAs) are those in which the band extrema associated with the gap are at the same point in momentum space. Excitation and de-excitation across the gap can occur via photons without the assistance of momentum-conserving excitations in the solid (namely phonons). Indirect gap semiconductors (e.g., silicon and germanium), on the other hand, have their band extrema at different points of crystal momentum in the Brillouin zone. The interband transitions in indirect gap semiconductors are phonon assisted and weakly radiative. Despite the phenomenal advances in silicon-based technology, which makes it an indispensable material in the computer industry, the indirect nature of its band gap has frustrated attempts by researchers to make silicon-based light-emitting diodes (LEDs) and lasers. On the other hand, gallium arsenide-based lasers and fast electron devices are readily available due to the GaAs direct band gap. Naturally occurring semiconductors, both direct and indirect, span a range of band gaps from the far infrared (IR) to the near ultraviolet (UV) regions of the electromagnetic spectrum. Solid solutions of two or more semiconductors often result in band gaps that vary continuously from that of one end member to the other. Figure 1 shows the band gaps of a number of elemental and compound semiconductors and their solid solutions versus their lattice constant at room temperature.

There are a number of novel techniques of crystal growth that have been developed in the past two decades that achieve band-gap tuning through artificial nanostructures. They employ techniques of material growth such as molecular beam epitaxy (MBE), chemical vapor deposition (CVD), and their variations. The resultant structures are laboratory made and do not occur in nature. It is the purpose of this article to discuss the physical properties and characterizations of these novel structures (1–3).

Following the initial proposal by Esaki and Tsu (4), a variety of nanoscale heterostructures of semiconductors of different band gaps have been fabricated. The thrust of this idea is to restrict the nearly free three-dimensional motion of electrons and holes in a crystalline semiconductor to two (quantum wells), one (quantum wires), or zero (quantum dots) dimensions by surrounding the semiconductor with a material that provides a potential barrier (usually another semiconductor). A quantum well (or wire or dot) is formed when the distance traversed by an electron or hole before it scatters becomes comparable to the width of the layer in which it resides. The charge carrier than "sees" the potential barrier, and its energy states become quantized. This alters the dispersion (energy versus momentum) relation and the density of states per unit energy of the new structure as compared with that of the parent semiconductor. The consequence is a drastic change in the effective band gap due to the additional quantum confinement energy.

In a quantum well, a typical structure consists of a sandwich of alternate barrier/well/barrier (B/W/B) layers. Quantum well systems are usually grown with several repeats: B/W/B/W/B/W . . ., with relatively wide barriers. When the barrier layers become narrow enough that the wave function of the charge carrier extends through the entire structure, the periodic structure is termed a "superlattice." In contrast to quantum wells, where the carrier wave function is principally confined to the layer of the potential well, leading to discrete energy states, superlattices have minibands and a dispersion relation of their own commensurate with their superperiodicity.

Superlattices with a monolayer thickness of two constituents can be thought of as a new crystal structure. They differ from three-dimensional compound semiconductors in that they are grown on substrates of specific orientation. Some substances are known to spontaneously grow into monolayer superlattices when deposited on specifically oriented substrates under certain growth conditions. These ordered, or self-organized, structures have tunable band gaps that depend on the degree of ordering (5).

If the lattice constants of the materials constituting the wells and barriers of the heterostructure are the same, the interfaces can maintain perfect atomic registry (pseudomorphic structures) without distorting the individual lattices. However, this is rarely the case (see Fig. 1). In lattice-mismatched semiconductors, the lattice constants of the constituents stretch or compress in order to maintain pseudomorphism. This leads to a biaxial strain in the individual layers. The strain splits the energies of heavy- and light-hole valence bands (which were degenerate in the parent semiconductor), the amount being dependent on the orientation, strain, and the materials of interest. Not only is the band gap altered but the nature of the band gap changes depending on whether the strain is compressive or tensile (6). For example, the tensile stress in the gallium antimonide (GaSb) layer makes the transition to the light-hole band lower in energy for the GaSb/AlSb quantum well system (which is desirable due to the larger mobility of the light hole), whereas the heavy-hole transition is lower in energy for bulk GaSb. While registry is maintained for thin layers, beyond a critical thickness strains due to lattice mismatch become too large to maintain pseudomorphism in a heterostructure. Defects and misfit dislocations relieve the strain at the expense of interface quality. The smaller the lattice mismatch, the larger is the critical thickness, a feature that is desirable in device fabrication.

External perturbations such as temperature, pressure (hydrostatic and uniaxial), and electric and magnetic fields further alter the band gaps of semiconductors and heterostructures. These perturbations are also useful in unraveling band

J. Webster (ed.), *Wiley Encyclopedia of Electrical and Electronics Engineering*. Copyright © 1999 John Wiley & Sons, Inc.

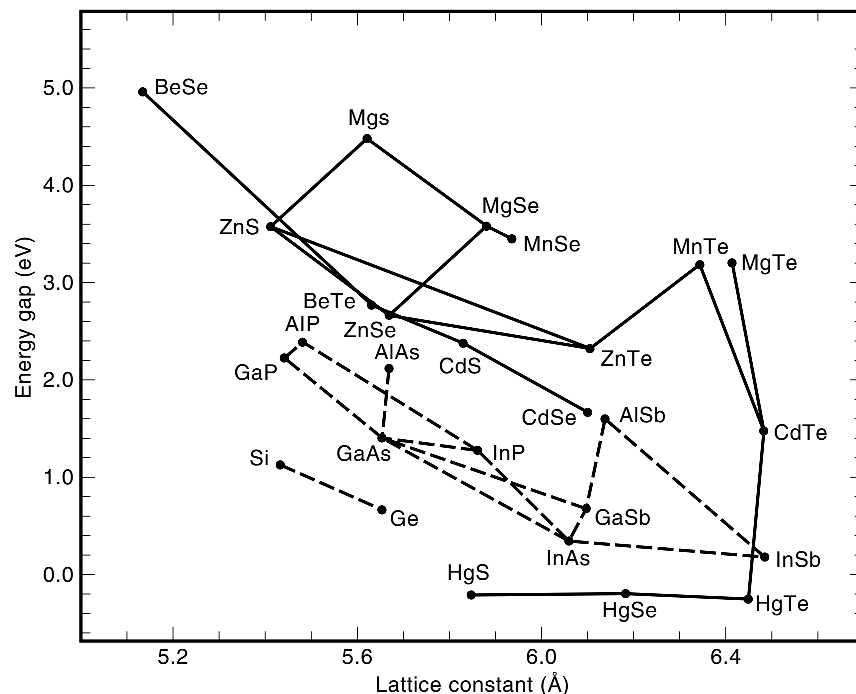

Figure 1. Band-gap energies versus lattice constants of semiconductors and their alloys at 300 K.

structural information, since band gaps corresponding to different wave vectors respond to the perturbations at different rates. Valuable information on band alignments, energies of confined states, and their mutual interactions have been elucidated from some studies (7–9).

BAND-STRUCTURE PROPERTIES OF BULK SEMICONDUCTORS

The energy states of electrons in a bulk semiconductor are described in terms of the propagation of nearly free electrons in the periodic potential of the crystal lattice. The electronic energy band structure describes the energy, E, versus the momentum wave vector, $\boldsymbol{k}$, for different bands. Figure 2 shows the band structure of GaAs as calculated by an empirical pseudopotential method (10). The symbols, Γ, X, and L refer to high symmetry points of $\boldsymbol{k}$ in the Brillouin zone corresponding to the zone center ($\boldsymbol{k} = \boldsymbol{0}$), [100], and [111], respectively. GaAs is a direct gap semiconductor with both the maximum of the valence band (Γ_8) and the minimum of the conduction band (Γ_6) at $\boldsymbol{k} = \boldsymbol{0}$. The effective mass of the electron m_e^* at the conduction band minimum, which represents the reciprocal of the curvature of the energy versus $\boldsymbol{k}$, is 0.067 m_e (m_e is the free electron mass). The valence bands consist of the heavy- and light-hole bands that are degenerate at the Γ point and the Γ_7 band split by the spin-orbit interaction. The valence bands are highly anisotropic. The conduction band minima along the X and L points are higher in energy than the Γ_6 minimum.

The band structure of aluminum arsenide (AlAs) looks very similar to that of GaAs with the following exception. The lowest conduction band minimum is close to the X point along [100] rather than at Γ. The band gap is *indirect.* In GaAs, the transition of an electron across the band gap could be accomplished by the absorption or emission of a photon. In AlAs, however, conservation of energy and momentum (wave vector) demand the participation of one or more phonons to assist the photon in transferring an electron from the conduction band minimum at X_6 to the valence band maximum at Γ_8. Due to the large lifetime of this process, the radiative transitions are very weak. In addition, the effective mass at the X_6 point is highly anisotropic, with a longitudinal and transverse effective mass, $m_l = 1.1\, m_e$ and $m_t = 0.2\, m_e$. A larger effective mass

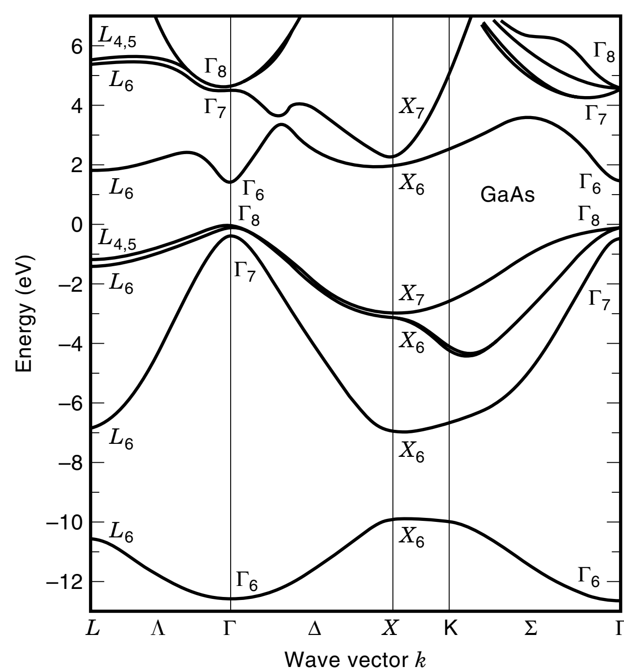

Figure 2. Electronic energy-band structure of GaAs along different high-symmetry directions of momentum space (from Chelikowsky and Cohen, Ref. 10). Reprinted with permission from the author.

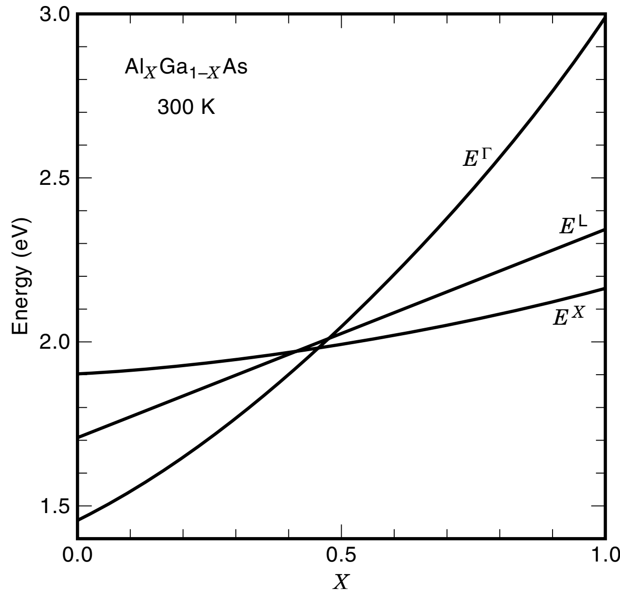

Figure 3. Room-temperature values of the energies of the Γ, *X*, and *L* minima as measured from the top of the valence band maximum of $Al_xGa_{1-x}As$ as a function of *x* (Refs. 12–14).

means a smaller mobility for the charge carrier, which limits transport phenomena.

The band structure of most III–V (e.g., GaAs, AlAs, GaP), II–VI (e.g., ZnS, ZnSe), and elemental group IV (Si, Ge) semiconductors with the zinc blende crystal structure have band diagrams similar to Fig. 2 (10). The values of various energy gaps such as $(\Gamma_6 - \Gamma_8)$, or the E_0 gap; $(\Gamma_6 - \Gamma_7)$, or the $(E_0 + \Delta_0)$ gap; $(L_6 - L_{4,5})$, or the E_1 gap; $(L_6 - L_6)$, or the $(E_1 + \Delta_1)$ gap and the nature of the fundamental gap (direct vs indirect) are different. These values are available in many handbooks (11).

As seen in Fig. 1, a large number of bulk semiconductors with band gaps ranging from the far infrared to the UV have been synthesized. The lines joining one material to the other in Fig. 1 indicate solid solutions whose band gaps can vary continuously from one end member to the other. As an example, the energies of the direct Γ, and indirect *X* and *L*, conduction minima as measured relative to the top of the valence band in solid solutions of GaAs and AlAs (referred to as $Al_xGa_{1-x}As$) are shown (12–14) in Fig. 3. Note the crossover from the direct to the indirect gap at $x \approx 0.4$.

CHANGES IN BAND STRUCTURE DUE TO CARRIER CONFINEMENT

Confinement of quasi-free electrons and holes in a semiconductor in zero, one, or two dimensions alters their energy structure drastically, leading to novel optical and electrical properties. Such structures are fabricated by modern epitaxial techniques. In this section, we discuss some of the properties of these structures from our understanding of the electronic band structure of the bulk materials and their modification due to quantum confinement.

Quantum Wells and Superlattices

Consider a situation as in Fig. 4 in which thin epitaxial layers of GaAs and AlGaAs are grown along the *z*-direction (usually on a GaAs substrate, which is not shown). Also consider the interfaces to be sharp and free of defects. The (direct) band gap of AlGaAs is larger than that of GaAs. A plot of the energies of the conduction and valence band edges as a function of *z* displays sharp discontinuities at the interface leading to potential wells for electrons (in the conduction band) and holes (in the valence band). The sum of the depths of the conduction and valence potential wells, ΔE_c and ΔE_v, should be equal to the difference in band-gap energy between AlGaAs and GaAs. The depth of each potential well, however, depends on the band alignment, which is specific to the interface. The fraction of ΔE_c or ΔE_v normalized to their sum is known as the band offset. Factors affecting this quantity and its experimental determination will be discussed later. Owing to their importance, a great deal of theoretical and experimental effort has been invested in the determination of band offsets. A comprehensive review can be found in the literature (3). At this point it is enough to recognize that the motion of electrons is restricted to GaAs in the *z*-direction while the slab is semi-infinite in the *x*–*y* plane.

This one-dimensional potential well (assume the barrier heights to be infinite, for a moment) leads to standing waves along *z* with de Broglie wavelengths, λ_n, and, consequently,

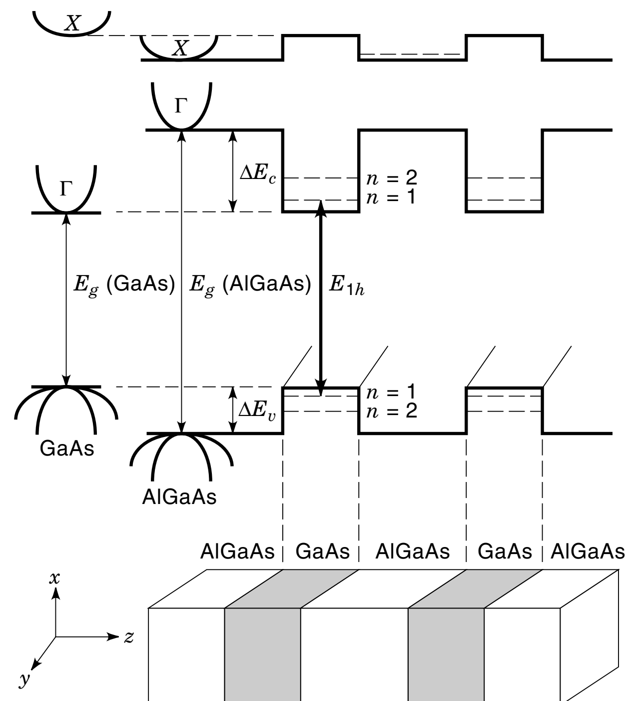

Figure 4. Schematic band alignment of the Γ, *X*, and the heavy-hole valence band extrema in thin slabs of GaAs and AlGaAs. The slabs are semi-infinite in the *x*–*y* plane, but the movement of carriers in the *z*-direction is confined to the potential wells in GaAs. This confinement leads to quantization of their energies. Note the type I alignment for the Γ conduction band for which the potential wells for electrons and holes are in GaAs. The *X* conduction band has a type II alignment so that electrons reside in the *X* well of AlGaAs and holes reside in GaAs.

discrete energies E_n for the carriers. The dispersion along the x- and y-directions is not affected, however.

$$\lambda_n = \frac{2L_z}{n}; \quad E_n = \frac{\hbar^2 k^2}{2m^*} = \frac{\hbar^2 \pi^2 n^2}{2m^* L_z^2}; \quad n = 1, 2, 3 \ldots \qquad (1)$$

The ground state for the electron and the hole in the well has been raised from the band edges to the corresponding $n = 1$ levels. The effective band gap is increased by the sum of the confinement energies for the electron and the hole given from Eq. (1). It is clear that the confinement energies increase as the well width, L_z, is decreased or n is increased.

Band alignment is usually classified as type I or type II. In type I alignment, the potential wells for both electrons and holes reside in the same material that forms the quantum wells. Type II alignment, on the other hand, has the potential wells for electrons in one material and holes in the other. Figure 4 schematically displays such an alignment for GaAs/AlGaAs quantum wells. Examples of type I alignment for the potential wells associated with the fundamental gaps are GaAs/AlGaAs, GaSb/AlSb, InGaAsP/InP and GaAs/GaP systems. GaAs/AlAs superlattices with very thin layers of GaAs can form a type II alignment. The large confinement energy of Γ electrons pushes the $n = 1$ state of Γ electrons higher in energy than the first confined state in the X well. One can achieve the same scenario by subjecting the GaAs/AlGaAs quantum wells to external hydrostatic pressure. In both type I and type II alignments, the conduction bands of both materials are separated from their valence bands by an energy gap. In some cases, however, the conduction band of one material may be *lower* than the valence band of the other material. Such systems are referred to as "misaligned." The InSb/GaSb system belongs to this class. Type I alignment is desirable and often results in very strong optical transitions via the recombination of excitons even at room temperature. The binding energy of the excitons increases rapidly for narrower well widths due to the increased two-dimensional nature (15). Type II excitons are generally weak due to their indirect nature. The recombination occurs across the heterointerface, thus being crucially limited by the interface quality. In short-period GaAs/AlAs superlattices, however, due to the folding of the component of the X band along the growth direction into the Γ point and the strong Γ–X mixing, type II transitions are pseudodirect and are very intense as a result of the high quality of MBE-grown materials.

Due to the lattice mismatch between the materials forming the heterostructures, the layers can be biaxially strained, the strain being compressive in one layer and tensile in the next. The substrate material can also define the strain in thin epilayers grown pseudomorphically to maintain registry. Strain splits and shifts band extrema. The amount depends on the band, the material of interest, and the direction and nature of the strain (16,17). Band offset determinations in strained layer heterostructures should take this additional effect into consideration.

In addition to changes in the energy levels due to quantum confinement, the density of states also changes from the smooth three-dimensional parabolic shape to a staircase-like function at each energy state for a quantum well. Figure 5(a–b) displays this effect.

The optical absorption spectrum in Fig. 6 for quantum wells of different well widths exhibits the features (18) predicted in Fig. 5(a–b). For a wide (4000 Å) well, the spectrum resembles that of a bulk semiconductor with a sharp exciton (bound electron hole pair) and the bulk density of states. For narrower wells, the absorption increases in steps with peaks corresponding to excitonic transitions between electrons and holes in different quantized levels. Due to the differences in heavy and light hole masses, the confinement energies for the holes corresponding to the same n are different. This leads to the removal of the degeneracy between heavy- and light-hole valence bands, and pairs of peaks appear for each n.

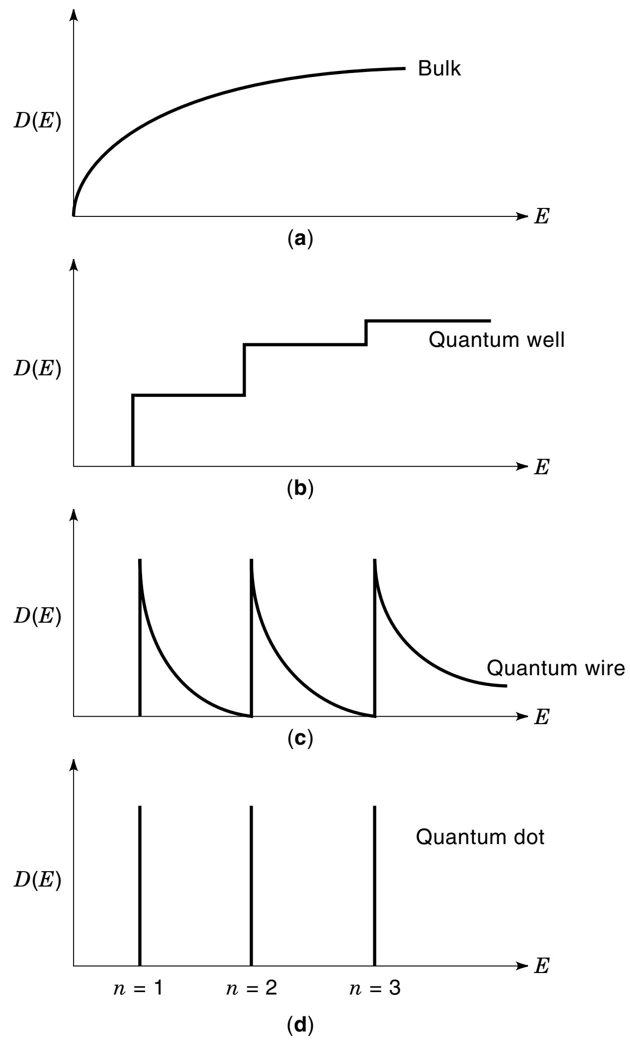

Figure 5. Density of states for (a) bulk, (b) quantum well, (c) quantum wire, and (d) quantum dot, in which the motion of electrons (holes) is restricted into three, two, one, and zero dimensions.

For quantum wells composed of direct band materials, such as GaAs, the oscillator strength of the transitions is very high, leading to very strong emissions with nanosecond radiative lifetimes. Development of low-threshold room-temperature lasers and nonlinear optoelectronic devices owe their existence to this property (19).

While Eq. (1) describes the qualitative features associated with quantum wells, exact calculation of energies requires realistic parameters. The assumption of an infinite barrier height quickly breaks down for larger n or shallow potential wells. An extension of the well-known "square potential well"

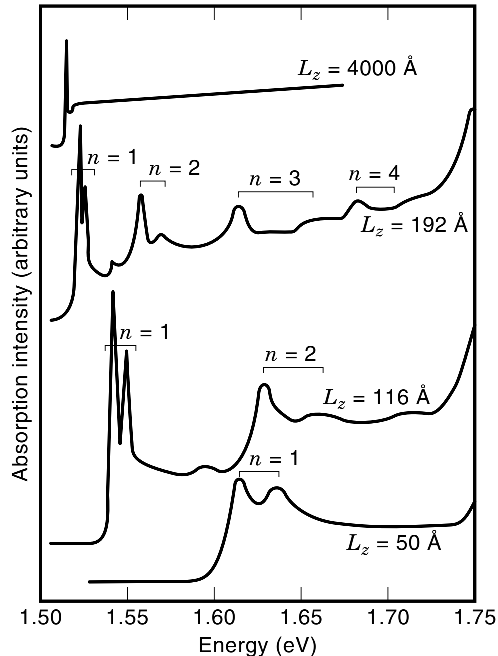

Figure 6. Optical absorption for quantum wells of different widths. The pairs of peaks correspond to excitonic transitions from the electron to heavy and light holes for each n. The steplike increase in the density of states is as expected. For a wide well, the spectrum resembles that of bulk GaAs (Gossard, Ref. 18). Reprinted with permission from the author.

problem in elementary quantum mechanics can yield insight into the solution of this system.

The simplest example is that of an electron confined in a potential well of depth ΔE_c. Figure 4 depicts this situation if the barrier widths are assumed to be large and the potential wells are decoupled. The Schrödinger equation can be written as

$$\left[-\frac{\hbar^2}{2m^*}\nabla^2 + \Delta E_c(z)\right]\Psi(z) = E\Psi(z) \tag{2}$$

Inside the well, the wave functions look similar to standing waves [characterized by the quantum number n of Eq. (1)], but the barrier wave functions die down exponentially with z. The boundary conditions require continuity of the well and barrier wave functions and their probability currents at the interface. This leads to a set of symmetric and antisymmetric solutions obtained by numerical or graphical methods. Using the one-band Wannier orbital model with appropriate material parameters (electron, hole masses, well widths, etc.), one can compute the energy levels of electrons and holes (20,21). Notice that the carrier mass and the depth of potential well in Eq. (2) should be appropriately changed to obtain the solutions for holes. After the electron and hole confinement energies E_e and E_h are obtained, the transition energies of the quantum well for a type I quantum well are given by

$$E_n = E_{g(\mathrm{well})} + E_e + E_h - E_{\mathrm{ryd}} \tag{3}$$

where E_{ryd} is the two-dimensional Rydberg (15). The E_{1h} transition shown in Fig. 4, for example, contains the confinement energies of the electron and the heavy hole for $n = 1$.

The picture is further complicated for the holes. Due to the anisotropy and mass differences, the hole bands corresponding to different n cross one another. The interaction between the bands leads to considerable hybridization and dispersion along the x–y plane (22,23).

A finite element method (FEM) has been found to yield accurate eigenvalues for bound state problems (24). In this method, the heterostructure layers are split up into a number of "cells," or elements, in each of which the physical considerations of the problem hold. The eigenvalue problem is set up in each element by assuming that the wave functions are given locally by fifth-order Hermitian interpolation polynomials, which have the property that the expansion coefficients correspond to the wave function and its derivatives at the nodes. The accuracy can be increased by employing more elements in the computation (25).

The analysis of a single quantum well can be extended to a set of coupled quantum wells. A well-known case is one of a periodic superlattice structure of alternating *thin* layers of two semiconductors with different band gaps. The so-called superlattice can be thought of as a structure in which the electron (or the hole) sees the periodic potential of a crystal lattice and the superlattice potential along the z-direction. The lattice constant of the superlattice, d, is an integral multiple of the lattice constants of the constituent materials (a). This results in folding the original Brillouin zone with edges at ($\pm\pi/a$) into mini-Brillouin zones with boundaries ($\pm\pi/d$). The number of minibands is given by the ratio (d/a) and the width by the coupling of the quantum well levels. The density of states differs from that of quantum wells [Fig. 5(b)] in that the steps are replaced by smooth curves.

An example of the FEM calculation for a 10-monolayer $Al_{0.31}Ga_{0.69}As$/18-monolayer GaAs superlattice shows the dispersion along and perpendicular to the growth direction (Fig. 7). Figure 8 shows the piezomodulated reflectivity spectrum of this sample, in which sharp signatures are observed for optical transitions from a critical point in the valence band to the conduction band (26). Most transitions are direct in nature between two M_0-type (extrema) or M_1-type critical points (saddle points).

The thicknesses of the two constituent materials constituting a superlattice critically determine the transition energies. This effect is dramatized in short-period superlattices of $(GaAs)_n(AlAs)_m$ (n monolayers of GaAs and m monolayers of AlAs), where n and m are of the order of 1 to 10. Returning to Fig. 4, if AlGaAs is replaced by AlAs, the potential wells for the electrons in the X conduction band of AlAs decrease in energy, thus rendering the type II energy lower than that of type I for $m = n < 13$. For asymmetric superlattices (unequal m and n), the layer thickness at which the crossover from type I to type II occurs depends on both n and m. Figure 9 shows a calculation of type I and type II transition energies as a function of n and m for n, m between 1 and 10 monolayers.

Quantum Wires and Dots

Further restriction of the motion of carriers into one dimension (say x) leads to quantization of energy levels in the other two directions. The dispersion relation would be parabolic for k_x only. The density of states appears as in Fig. 5(c). Quantum dots are essentially mesoscopic particles with no dispersion.

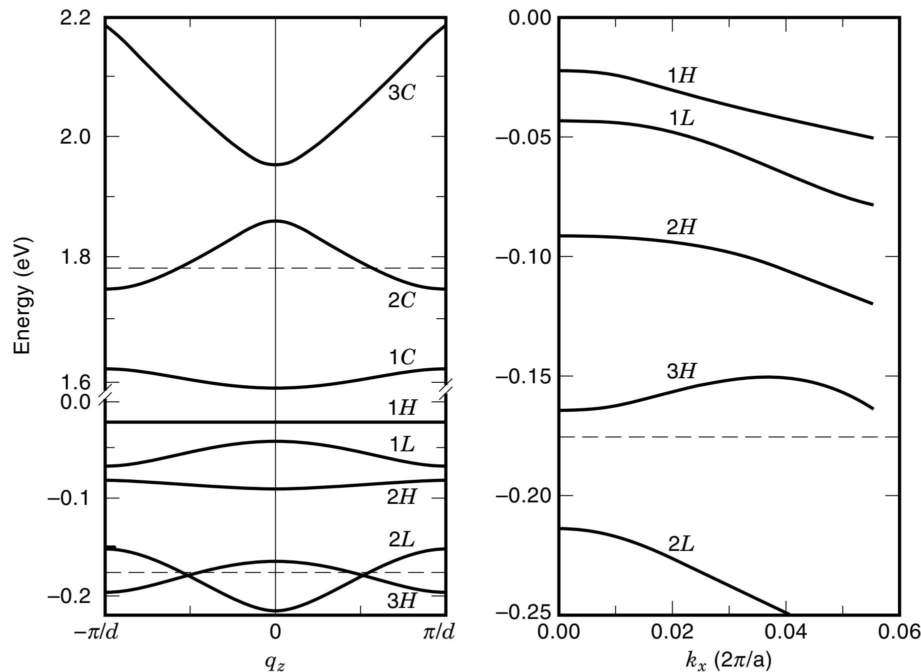

Figure 7. The dispersion along (left panel) and perpendicular to (right panel) the growth direction of a $(GaAs)_n(Al_{0.31}Ga_{0.69}As)_m$ superlattice. Number of monolayers: $n = 18$ and $m = 10$. The energies are measured relative to the valence band edge of GaAs. The dashed lines indicate the energy of the band edges of $Al_{0.31}Ga_{0.69}As$ (Parks et al., Ref. 26). Reprinted with permission from the author.

The density of states would have delta function singularities at the energies [Fig. 5(d)].

FABRICATION OF SEMICONDUCTOR HETEROSTRUCTURES

Modern epitaxial techniques of MBE and vapor-phase epitaxy (VPE) have enabled researchers to realize the type of novel structures described earlier. There are a number of good technical review articles on this subject (27,28). We briefly outline the salient features.

Ultra-thin layers of semiconductors with precise control over their thickness, composition, and doping levels are possible with these techniques. In MBE, elemental sources in the gas phase are used. The process is free of by-products and only the gas–substrate interaction is important. The deposition of layers can be monitored in situ via reflection high-energy electron diffraction (RHEED) and reflectance difference spectroscopy (RDS). The basic processes of metal organic VPE (MOVPE) involve gas phases with complex compounds as precursors leading to fabrication of complex ternary and quaternary compounds. A typical MBE system consists of a

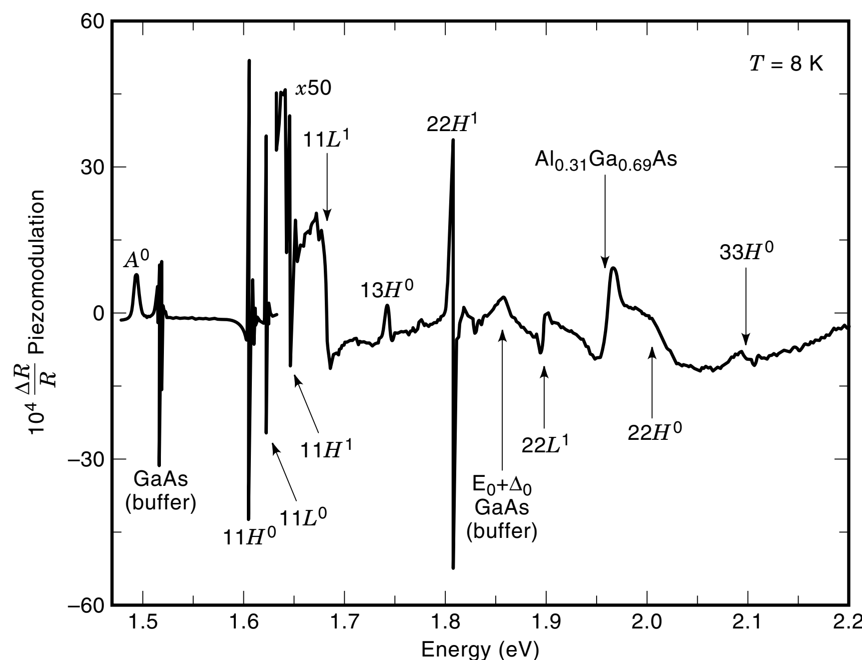

Figure 8. The piezomodulated reflectivity spectrum of the sample shown in Fig. 7. The transitions originate across the valence and conduction subbands of the sample. The superscripts 0 or 1 indicate transitions at the critical points $q_z = 0\,(M_0)$ or $q_z = 1\,(M_1)$, respectively (Parks et al., Ref. 26). Reprinted with permission from the author.

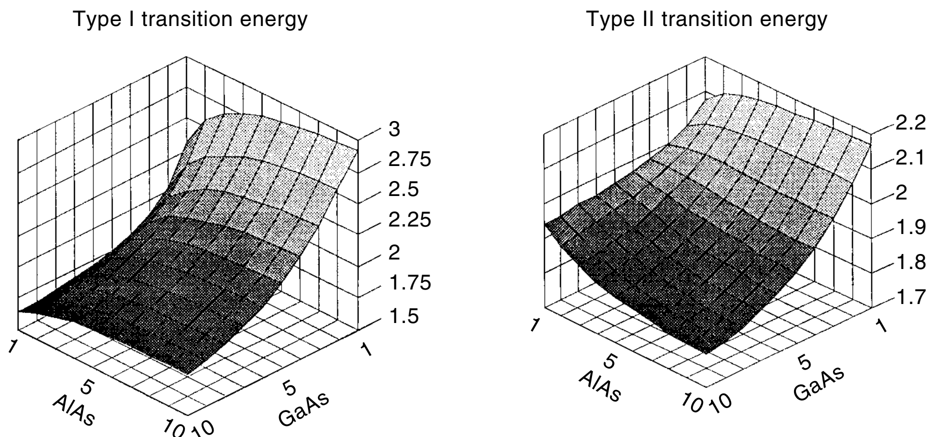

Figure 9. Type I and type II energies of a $(GaAs)_n(AlAs)_m$ superlattice for $n, m = 1, 10$. In this three-dimensional plot, the axes correspond to the number of monolayers of GaAs and AlAs and the transition energy in electronvolts. Notice that the lowest energy can be of type I or type II for asymmetric combinations of m and n. For $n = m \leq 13$, the superlattice is type II.

chamber under ultra-high vacuum, equipped with effusion cells for sources, shutters with computer control, and the substrate with a rotating holder with temperature control. The MOVPE process involves pyrolysis of vapor-phase mixtures of the compounds of interest and hydrogen carrier gas. Doping is accomplished by introducing gaseous reactants into the gas flow. The MOVPE systems consist of gas-handling systems with source metalorganics and hydrides, instruments necessary to control gas flows, a reaction chamber in which pyrolytic reaction and deposition takes place, and various exhaust and plumbing lines.

Lateral patterning techniques such as electrostatic squeezing, lithographically defined deep-mesa etching, and focused ion-bean writing are used in fabrication of quantum wire and dot structures.

The characterization techniques include the following. High-resolution transmission electron microscopy (HR TEM) gives detailed information of the atomic arrangement at the interface in limited microscopic areas, and is destructive. High-resolution X-ray diffraction is a nondestructive technique and is used extensively. Photoluminescence (PL), absorption, modulated reflectance, Raman scattering, and electro-absorption are some of the optical techniques that probe various properties.

EFFECT OF EXTERNAL PERTURBATIONS

Temperature

The band gaps of semiconductors generally decrease with increasing temperature and are commonly described by a semi-empirical relationship (29):

$$E_g(T) = E_g(0) - \frac{\alpha T^2}{\beta + T} \tag{4}$$

Here, α and β are constants. Besides the changes due to the thermal expansion of the lattice, the band-gap changes are due to electron–phonon interactions and phonon self-energy terms (30). The values for α and β from Eq. (4) that were determined from experimental data for different semiconductors are available in the literature (3,11). The temperature dependence of quantized states associated with the direct gap of GaAs in GaAs/AlGaAs quantum wells (31,32) is essentially the same as that of bulk GaAs (33). The values are $\alpha = (5.4)10^{-4}$ eV/K and $\beta = 204$ K.

Hydrostatic Pressure

The application of high pressure in the investigation of the vibrational and electronic properties of bulk semiconductors and their alloys goes back to the early days of the introduction of the diamond anvil cell (34). The unique manner in which different band extrema of a bulk semiconductor respond to pressure provides a diagnostic tool of electronic states whose properties closely resemble the band extrema they are associated with. The donor and acceptor states of effective-mass–type shallow impurities belong to one class of such states. The energy states of electrons and holes in quantum well heterostructures (QWHs) and superlattices (SLs) are the second class of such systems. This section deals with the latter. While the resemblance to the bulk bands forms a source of their identification and characterization, the deviations help us understand properties of the heterostructures themselves, such as the effects of quantum confinement, interfacial strains, and mixing between subband states (7–9,35).

Band Alignment Problem. Research showed early on that the band alignments of GaAs and $Al_xGa_{1-x}As$ were such that potential wells were formed for the electrons in the conduction band and the holes in the valence band in GaAs layers at the zone center (Γ point). The depths of the potential wells depend on the difference between the band gaps of the materials forming the potential well and the fraction of that difference that went into the conduction and valence band wells. While the sum of the depths of the potential wells was accurately known, the depths of individual wells were not. Excitonic transitions from the confined states of electrons to those of the holes result in strong and well-defined signatures in photoluminescence, photoreflectance (PR), and excitation spectroscopies. Due to the mass difference, the energies of confined states of light holes and heavy holes are different, leading to two sets of transitions from electrons to heavy and light holes, respectively. The energies of the confined states can be readily computed by models already described that incorporate the masses of the charge carriers, widths of potential wells, and their depths (which is the only unknown quan-

tity). The experiments listed previously determine the *sum* of the confinement energies of the electron and the hole, but not individual values. This problem led to estimations of the fractional band offset of the potential well for electrons to be widely different. Theoretical and experimental estimations ranged from 0.86 to 0.5. A direct experimental determination of this important quantity without the pitfalls of models based on many parameters was crucial. In the next section, we show how hydrostatic pressure studies provided a direct and convincing answer to this question.

Let us return to Fig. 4, which shows a schematic band alignment of a GaAs/$Al_xGa_{1-x}As$ quantum well structure. ΔE_c and ΔE_v are the depths of the electron and heavy hole potential well (the light hole is not shown). Also shown in the figure are the potential wells for the X minima along (100). Notice that the band alignment is such that the potential well for X is in $Al_xGa_{1-x}As$. Generally, these bands, whose energy is larger than those related to the direct gap (Γ), do not play any significant role at ambient pressures and for small x. However, under hydrostatic pressure, the direct gaps of GaAs and $Al_xGa_{1-x}As$ increase rapidly (10.7 meV/kbar for GaAs) and the X gaps reduce at a moderate rate (-1.3 meV/kbar for GaAs). At a certain pressure P_c, the Γ and X bands cross. For $P > P_c$, the X wells have lower energy and the transition denoted E^x becomes observable. Figure 10 shows this situation.

The E^x transition is from the electron in the $Al_xGa_{1-x}As$ to the hole in the GaAs across the interface. Casual observation suggests that the depth of the valence potential well can be determined from a knowledge of the energy of the X gap in $Al_xGa_{1-x}As$ (denoted by E_g^x) and subtracting E^x from it. Corrections for the confinement energies of the X electron, heavy hole, and the exciton binding energy should be applied to refine the value. For wide wells, these corrections are minimal. This technique provides a direct experimental determination of the band offsets at the given pressures (36–39). Figure 11 shows the data from one such measurement. Due to the nearly identical pressure coefficient of the E^x transition and the X minimum of GaAs, the band offset ratio is nearly independent of pressure and has a value of $0.67:0.33$ for $\Delta E_c : \Delta E_v$.

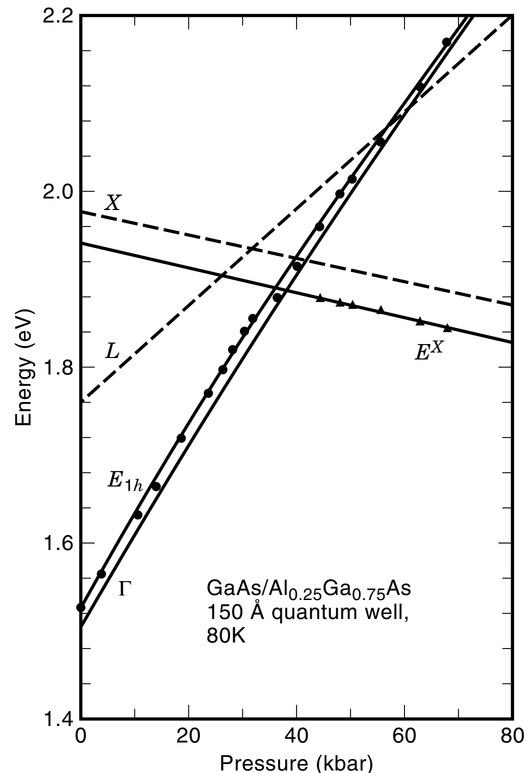

Figure 11. Pressure dependence of the E_{1h} and E^x transitions (see Figs. 4 and 10). The pressure dependence of the Γ, L, and X band edges of bulk GaAs are shown in the figure (Refs. 35 and 36).

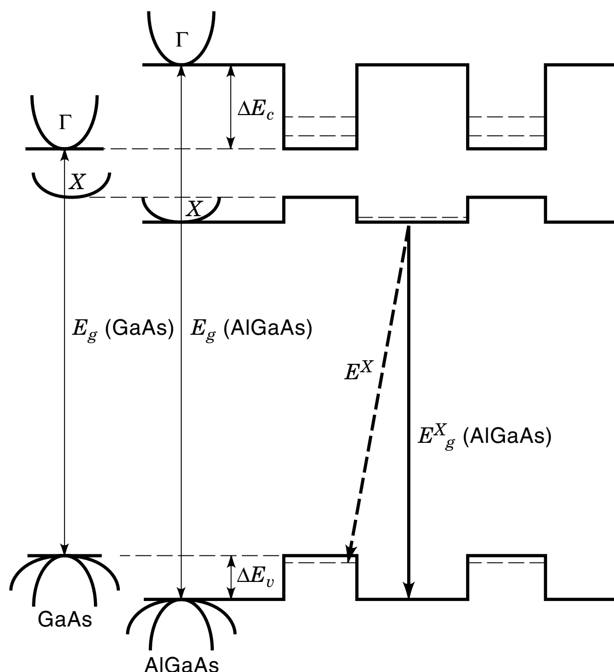

Figure 10. Schematic band alignment of the Γ, X, and the heavy-hole valence band extrema of a GaAs/$Al_xGa_{1-x}As$ quantum well under external hydrostatic pressure P. The Γ and X bands cross at a pressure P_c, which depends on the well width. For $P > P_c$, the energy of electrons in the X well of AlGaAs is lower than those in the Γ well of GaAs, and the type II transition E^x becomes observable.

The observation of E^x is a testimony to the interface quality of these heterostructures. The so-called type II transition can be observed at ambient pressures as the dominant peak in $(GaAs)_n(AlAs)_m$ short-period superlattices for $m = n < 13$. Here, n and m denote the number of monolayers of GaAs and AlAs, respectively. Moreover, the folding of the X point to the zone center builds a large density of pseudodirect states for short-period superlattices, leading to a bright zero phonon transition. The pressure studies once again determine the character of the bands they are derived from (40,41). The lifetimes of electrons associated with the type I, type II transitions and the scattering from Γ to X are 310 ps, 1 ns, and 310 fs, respectively. These values are obtained from the relative intensities of photoluminescence peaks versus pressure data and are consistent with the time-resolved measurements.

Quantum Confinement Effects. The energies of the subbands in a quantum well heterostructure are determined by parameters such as the carrier effective mass, m^*, the depth of the potential well, the well width, L_z, and the quantum number, n, as seen in Eq. (1). Pressure affects these parameters, so

that the pressure dependence of the QWH subbands is different from that of the bulk materials that constitute the well and the barrier. For deep wells and subbands close to the bottom of the well (wide wells), it is reasonable to expect the pressure rate of change of energy (pressure coefficient), α, of the subband to be close to the α of the bulk well material. For narrower wells and higher lying transitions, however, the spillover of the wave function into the barrier causes the subbands to exhibit an α that is affected by the well and the barrier.

There are several competing effects on α in a QWH. For a complete calculation, all the effects have to be considered in a consistent fashion. The effect of pressure on the subbands is described in detail in Ref. 7, which we summarize here.

1. The decrease in the well width, L_z, with pressure leads to an increase in the confinement energy and a consequent increase in α. For structures grown on (100)-oriented substrate, this decrease is given by the theory of elasticity:

$$L_z(P) = L_z(0)[1 - (S_{11} - 2S_{12})P] \tag{5}$$

   where P is the magnitude of the external hydrostatic pressure and S_{11} and S_{12} are the elastic compliance constants of the well material. While this is the most obvious effect, it is $\sim$0.1% in GaAs, and is usually much smaller than other effects.
2. The well and barrier, in general, have different (bulk) pressure coefficients. In the prototype $GaAs/Al_xGa_{1-x}As$ case, $\alpha_{GaAs} = 10.7$ meV/kbar, while $\alpha_{Al_{0.3}Ga_{0.7}As} = 9.9$ meV/kbar (Ref. 7), so that the depth of the potential well decreases with pressure, thereby depressing the subband energies and the pressure coefficient.
3. The increase in the energy of the direct gap with pressure leads to an increase in the effective mass of electrons and holes in both well and barrier. This decreases the confinement energies and the α's.

   Lefebvre et al. (42) have used the three-band $\mathbf{k}\cdot\mathbf{p}$ model (43) to calculate the change in the effective masses with pressure. The effective masses contain terms involving the pressure-dependent fundamental gap and its spin-orbit split counterpart. Since the confinement energies change with the pressure-dependent effective masses, a consistent calculation of the effective masses is necesary (21). In the $GaAs/Al_xGa_{1-x}As$ system, the increase in the effective masses decreases the confinement energies, consequently decreasing the pressure coefficients of the subbands. The change in the effective masses is one of the dominant factors in the relatively smaller band-gap well materials such as GaAs, GaSb, and, perhaps, $In_xGa_{1-x}As$. It plays a relatively smaller role in wide gap materials such as $Zn_{1-x}Cd_xSe$.
4. The binding energy of the exciton depends directly on the effective mass, the static dielectric constant, and the well width. For bulk materials, the pressure dependence of the Rydberg can be written as

$$\frac{R^*_{3D}(P)}{R^*_{3D}(0)} = \exp(2\kappa P)\frac{\mu(P)}{\mu(0)} \tag{6}$$

   where the change in the dielectric constant is expressed as $\kappa = (1/\epsilon)(\partial\epsilon/\partial P)$, and $\mu(P)$ and $\mu(0)$ are the reduced masses of the excitons. This expression has to be suitably modified for two-dimensional excitons in very narrow wells.
5. The overlap of the subband wave function with the barrier will increase or decrease α, depending on whether the bulk pressure coefficient of the barrier is larger or smaller than that of the well. These effects are pronounced for narrow wells and higher subband transitions, where the wave function penetrates far into the barrier.
6. In strained layer superlattices, the interlayer strain between well and barrier changes with pressure due to the difference in the compressibilities of the two layers. This changing uniaxial strain affects the splitting of the heavy hole–light hole valence band edges, which in turn is reflected in the α's.

   In order to unravel the many competing effects that determine the dependence of α on L_z, it is crucial to measure the α's of all well widths in one single run or in a single sample containing isolated single quantum wells of different L_z grown on the same substrate. Figure 12 shows photoluminescence spectra at different pressures for such a sample containing 26, 48, 70, and 96 Å GaAs wells separated by 750 Å $Al_{0.33}Ga_{0.67}As$ barriers (37). The peaks shown as A, B, C, and D are the E_{1h} excitonic transitions. The weaker E_{1l} (electron to light hole) transitions were observed on an expanded scale (not shown) and at higher temperatures.

Detailed calculations include the various competing effects that lead to the variation of α with L_z, and we find excellent agreement with measurements. A calculation using a one-band Wannier orbital model and the slab method performed by Ting and Chang (21) is shown in Fig. 13. In GaAs/AlGaAs, the increase in effective mass plays the dominant role for wide wells, while wave function overlap dominates for narrow wells. Figure 13 also shows the changes expected for higher subbands: for a narrow well, large differences are expected in the α's of different subbands, largely due to the greater penetration of the subband wave function into the barrier as n increases.

While PL measurements yield information about the lowest subbands, emission from higher subbands is weak due to thermalization effects. In contrast PR can yield strong signals for a large number of subbands, even at 300 K, due to the derivative nature of the spectrum, which enhances the signal at the expense of background features. This enables one to study the quantum confinement effects as a function of subband index n at a fixed L_z. Figure 14 shows the energies of a number of transitions observed as a function of pressure using PR in a GaSb/AlSb QWH at 300 K (44). The higher lying transitions move with smaller pressure coefficients due to the increased quantum confinement effect.

Intervalley Scattering Rates. The scattering of electrons from a low-mass Γ valley to larger mass L and X valleys, leading to negative conductance, is important in the Gunn effect. The strength of this mechanism is described by the intervalley deformation potential (IDP) constant. A number of theoretical

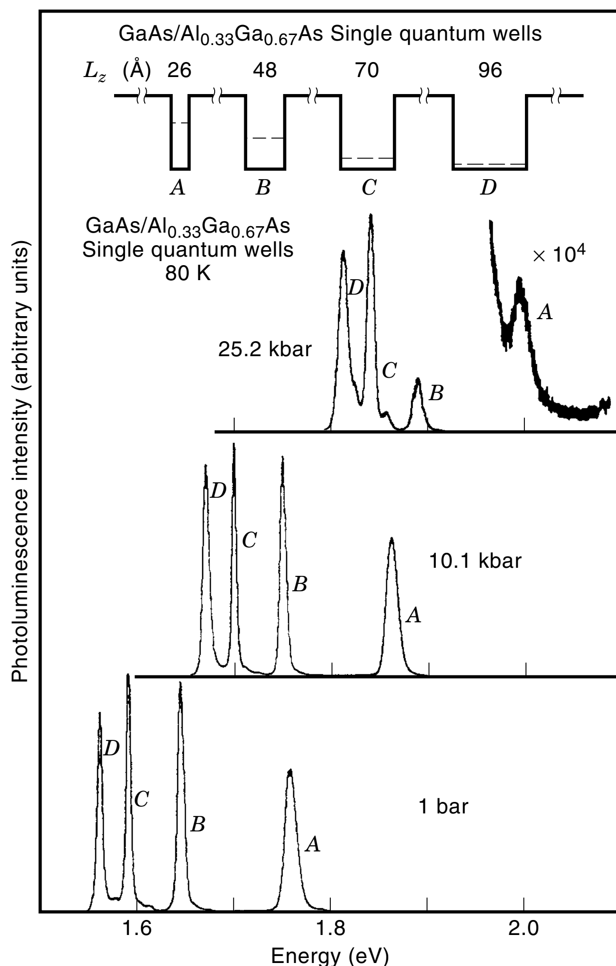

Figure 12. The E_{1h} transition (across the first quantized states of electron to heavy hole) of a sample containing isolated quantum wells of GaAs of widths 26, 48, 70, and 96 Å, separated by 750 Å wide $Al_{0.33}Ga_{0.67}As$ barriers. Under pressure, the peaks move up in energy as the band gap increases. The rate of movement, α, depends on the well width due to quantum confinement effect (Venkateswaran et al., Ref. 37).

models based on empirical pseudopotential or tight-binding schemes have calculated this important quantity. A dependence of the IDP on the phonon wave vector resulting in a temperature dependence of the IDPs is described by Zollner et al. (45). Figure 15 compares a calculation based on the rigid pseudopotential method with hot-electron luminescence measurements.

Satpathy et al. (35) have deduced the intervalley scattering rates by a detailed analysis of the pressure dependence of the type I exciton in $GaAs/Al_xGa_{1-x}As$ quantum wells. The linewidth of the type I transition remains constant until the Γ–X crossover and increases rapidly with pressure. This effect has been interpreted as being due to scattering of electrons from Γ to intervalley X (and L) electrons. The value for the IDP for Γ–X scattering deduced from these data is 107 ± 7 eV/nm. The value for Γ–L scattering is 65 ± 15 eV/nm.

Uniaxial Stress

The effect of uniaxial stress on the band edges of bulk GaAs has been studied extensively (46). Due to quantum confinement, a deviation from the bulk behavior (47–49) is expected, which should increase with decreasing well width. For stress along (100), perpendicular to the growth direction, Jagannath et al. (47) found the light-hole transitions to have smaller stress-induced shifts than the bulk GaAs, whereas the heavy-hole transitions had larger shifts than their bulk counterparts. A model based on the envelope function approximation describes the data well (50).

GaAs/AlAs superlattices display additional spectral features due to the anisotropy of the X conduction band valleys. For structures grown on (001)-oriented substrates, the longitudinal component of the X band (X_z) produces a folded pseudodirect state. The transverse components X_{xy} would produce indirect transitions, which are weakly allowed due to interface disorder. They are also observed via phonon-assisted transitions. The transition energy from the X_z state is lower in energy than that from the X_{xy} state due to its heavier mass and, consequently, smaller confinement energy. The lattice mismatch between GaAs and AlAs for superlattices grown on GaAs substrates produces a small biaxial compression in the AlAs layers, thus lowering the X_{xy} state compared with X_z. However, this effect is not sufficient to bring X_{xy} below X_z.

Recent uniaxial studies of GaAs/AlAs superlattices grown along (001) have shown (51) that for compression along (100), the X_{xy} state splits into two levels (Fig. 16). Unlike the X_y level, the X_x moves down in energy with stress and crosses the X_z at 3.2 kbar. The X_x transition is strictly forbidden but is weakly observed due to interface disorder. Several phonon-assisted recombinations of X_x are also seen at lower energies.

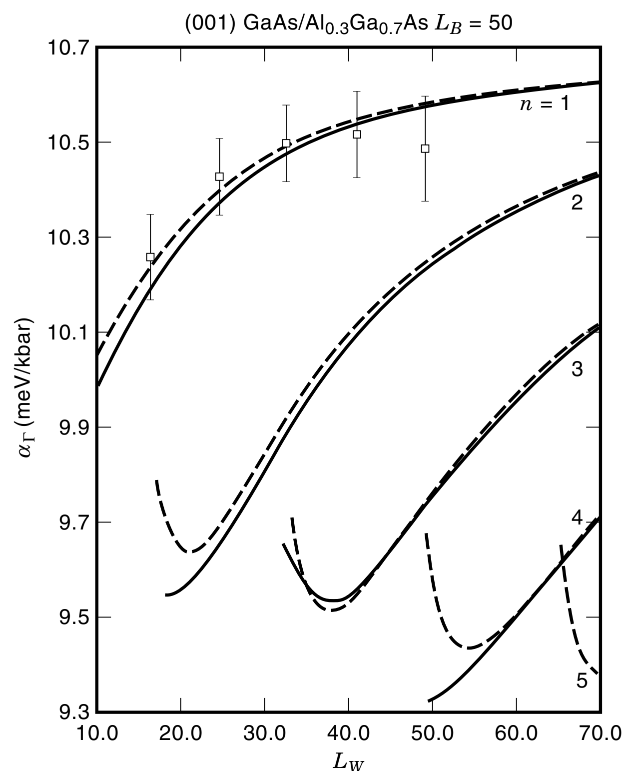

Figure 13. The well-width dependence of pressure coefficient α for excitonic transitions E_{nh} $(n = 1, 4)$. The calculation is by Ting and Chang (21) and the data are from Venkateswaran et al., Ref. 37. Reprinted with permission from the authors.

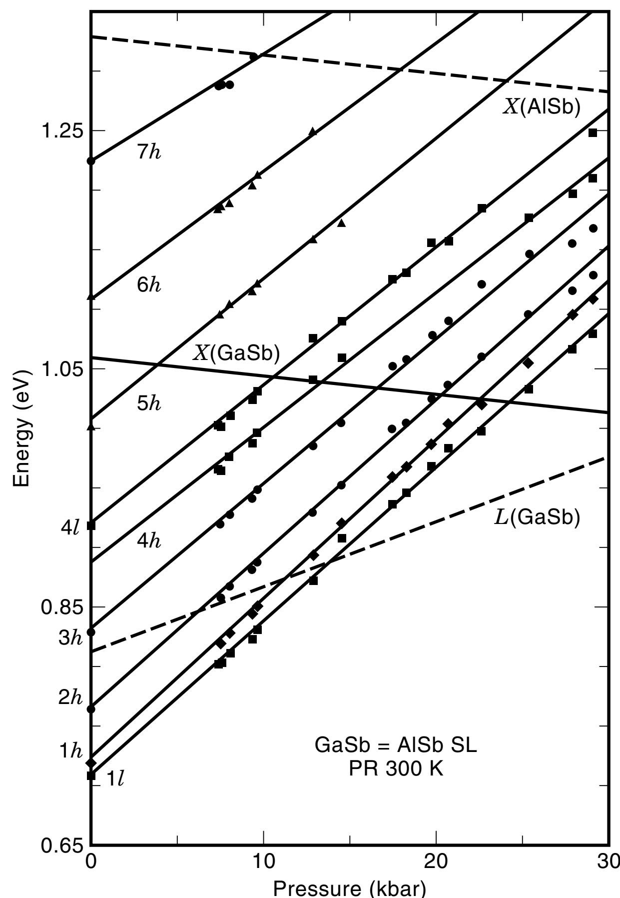

Figure 14. The pressure dependence of several quantized transitions in GaSb/AlSb quantum well heterostructure. The X and L band minima of GaSb and the X minimum of AlSb measured from the top of GaSb valence band are also shown. The decrease in pressure coefficients α with increasing quantum number is obvious (Rockwell et al., Ref. 44).

By studying these phonons via resonant Raman scattering, the authors assign them to the AlAs transverse acoustic (TA) at the X, GaAs longitudinal optic (LO) at X, and AlAs interface mode, respectively. In the absence of stress, a strong X_z transition that is pseudodirect is observed with rather weak phonon-assisted transitions. The phonons associated in this case are the longitudinal acoustic (LA) and LO of AlAs at X and possibly a GaAs interface phonon (52).

Electric Field

Excitons in bulk semiconductors exhibit shifts and broadening due to applied electric fields. At moderate fields, a small Stark-effect-induced red shift is observed. At larger fields, a blue shift and a quenching of the photoluminescence is seen due to mixing with the continuum states (53). The excitons associated with quantum wells have larger binding energies and their response to electric fields is very different. The quantum-confined Stark effect is rather strong in type I systems, leading to large red shifts (54). The electric field separates the electrons and holes at opposite corners of the quantum well, resulting in a decrease of the overlap of their wave functions. Type II systems, on the other hand, show an opposite behavior (55). A GaAs/AlAs superlattice with type II band alignment was examined under electric field by Meynadier et al. (56), who found that the X-related transition exhibited a large blue shift, leading to an anticrossing of the Γ transition at 45,000 V/cm. The Γ–X mixing potential was estimated to be a few millielectronvolts and decreased rapidly with increasing thickness of the AlAs barrier.

Analogous to the effect in bulk semiconductors, the band-to-band transitions are also affected by the Franz–Keldysh effect (57). Photocurrent spectroscopy of AlGaAs/GaAs quantum wells at large electric fields shows the appearance of forbidden transitions that exhibit large Stark shifts (58).

Superlattices with narrow barriers have their energy states extended in minibands. The wave functions of electrons and holes extend over many wells. For an applied electric field along the growth direction (z), the electron wave function tends to localize over a few wells. The blue shift depends on the miniband width and the superlattice period. Satellite

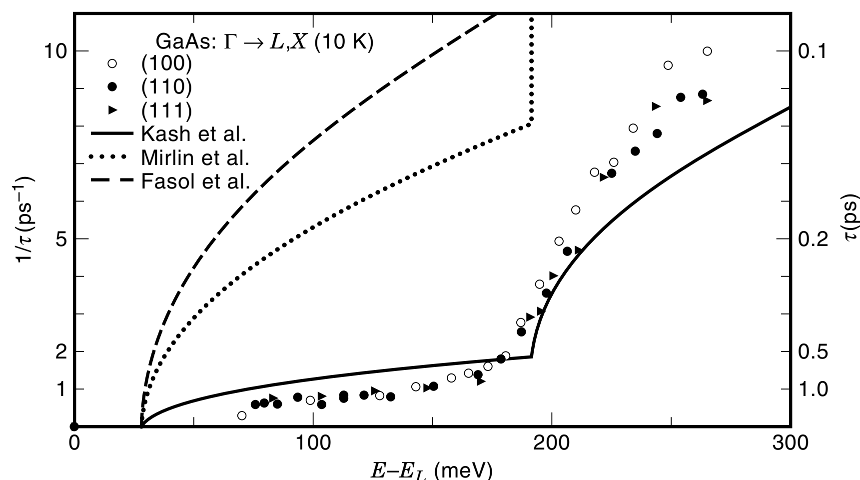

Figure 15. Intervalley scattering rates for GaAs obtained from the rigid-pseudoion method (symbols) compared with the hot-electron luminescence measurements (see Zollner et al., Ref. 45). Reprinted with permission from Elsevier Science.

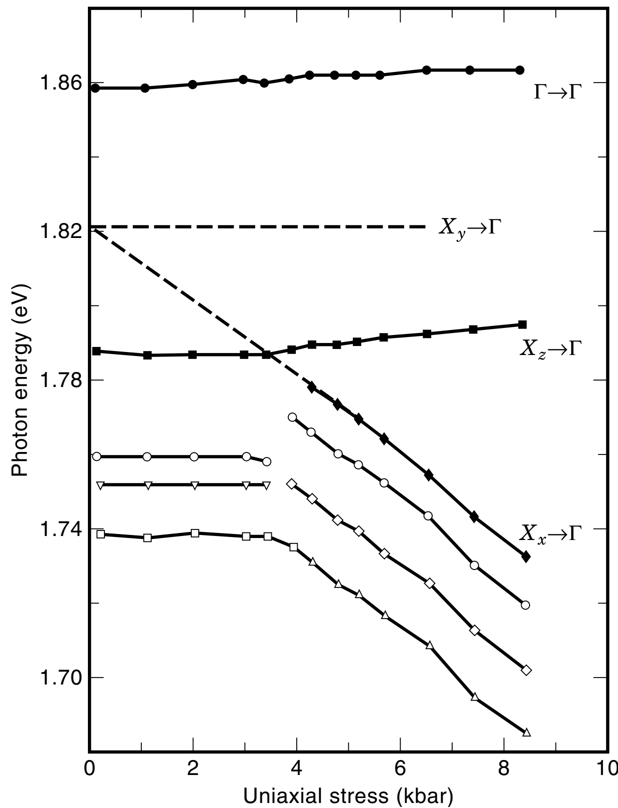

Figure 16. Uniaxial stress dependence of type I (Γ to Γ) and type II (X_z to Γ) transitions in a GaAs/AlAs superlattice. The X_{xy} level splits under stress and the X_x moves down in energy to cross X_z at 3.2 kbar. Open symbols denote phonon-assisted transitions (Tribe et al., Refs. 51 and 52). Reprinted with permission from Elsevier Science.

peaks (Stark ladder) are seen shifted from the main transition involving a localized hole and several electron levels. A description of the Wannier–Stark localization in semiconductor superlattices can be found in a review by Bastard et al. (59).

CONCLUDING REMARKS

We have outlined some basic properties of semiconductors and the heterostructures composed of them. Various aspects affecting the band gaps of these structures are discussed. Heterostructures based on III–V semiconductors, the GaAs/AlGaAs system in particular, are addressed at some length. Advances in materials technology are expected to bring forth new results on quantum wires, dots, and self-organized structures. We hope the sources given in this article (1–8,60,61) will supplement topics not discussed here.

ACKNOWLEDGMENTS

One of us (H.R.C.) thanks the Office of Research, University of Missouri-Columbia for a research leave during 1996–1997. He also appreciates the hospitality of Prof. A. K. Ramdas, Physics Department, Purdue University, where part of the work was done. He also acknowledges support by the NSF under grant DMR-9633107. M.C. thanks the U.S. Army for support through grant DAAL03-92-0381. Figure 1, including the most recent data available in the literature, was prepared by Ralf Vogelgesang.

BIBLIOGRAPHY

1. C. Weisbuch, In *Semiconductors and Semimetals,* vol. 24, R. Dingle (ed.), New York: Academic Press, 1986.
2. E. O. Gobel and K. Ploog, *Progr. Quant. Electron.,* **14**: 289–356, 1990.
3. S. Adachi, *GaAs and related materials.* In *Bulk Semiconducting and Superlattice Properties.* Singapore: World Scientific, 1994.
4. L. Esaki and R. Tsu, IBM *J. Res. Develo.* 61–65 (1970); *Appl. Phys. Lett.,* **22**: 562, 1973.
5. S. H. Wei and A. Zunger, *Phys. Rev. B,* **39**: 3279, 1989; *Appl. Phys. Lett.* **56**: 662, 1990; *Appl. Phys. Lett.* **58**: 2684, 1991.
6. C. G. Van de Walle, *Phys. Rev. B,* **39:** 1871, 1989.
7. M. Chandrasekhar and H. R. Chandrasekhar, Electronic transitions in semiconductor quantum wells and epilayers under pressure. *J. High Pressure Res.,* **9**: 57–82, 1992.
8. M. Chandrasekhar and H. R. Chandrasekhar, Optical studies of strained pseudomorphic semiconductor heterostructures under external pressure, *Philo. Mag. B,* **70**: 369, 1994.
9. H. R. Chandrasekhar and M. Chandrasekhar, Photoreflectance studies of electronic transitions in quantum well structures under high pressure, *SPIE, Modulation Spectrosc.,* **1286**: 207–220, 1990.
10. J. R. Chelikowsky and M. L. Cohen, *Phys. Rev. B,* **14**: 556, 1976.
11. *Landolt-Bornstein Numerical Data and Functional Relationships in Science and Technology,* Group III, vol. 22, O. Madelung (ed.), Berlin: Springer, 1987.
12. H. C. Casey Jr. and M. B. Panish, *Heterostructure Lasers.* New York: Academic Press, 1978.
13. H. J. Lee, L. Y. Juravel, J. C. Woolley, and A. J. Spring-Thorpe, *Phys. Rev. B,* **21**: 659, 1980.
14. A. K. Saxena, *Phys. Status Solidi,* **B105**: 777, 1981.
15. R. L. Greene, K. K. Bajaj, and D. E. Phelps, *Phys. Rev. B,* **29**: 1807, 1984.
16. C. G. Van de Walle, *Phys. Rev. B,* **39**: 1871, 1989.
17. F. H. Pollak, *Strained-layer superlattices: Physics.* In *Semiconductors and Semimetals,* vol. 32, T. P. Pearsall (ed.), Boston: Academic Press, 1990.
18. A. C. Gossard, Molecular beam epitaxy of superlattices in thin films. In *Thin Films: Preparation and Properties,* K. N. Tu and R. Rosenberg (eds.), New York: Academic Press, 1983.
19. R. D. Dupuis, P. D. Dapkus, N. Holonyak Jr., E. A. Rezek, and R. Chin, *Appl. Phys. Lett.* **32**: 295, 1978; D. A. B. Miller, *Surface Sci.,* **174**: 221, 1986.
20. W. T. Masselink, P. J. Pearah, J. Klem, C. K. Peng, H. Morkoc, G. D. Sanders, and Y. C. Chang, *Phys. Rev. B,* **32**: 8027, 1985.
21. D. Z.-Y. Ting and Y. C. Chang, *Phys. Rev. B,* **36**: 4359, 1987.
22. R. Eppenga and M. F. H. Shuurmans, *Philips Tech. Rev.,* **44**: 137, 1988.
23. M.-P. Houng, Y. C. Chang, and W. I. Wang, *J. Appl. Phys.,* **64**: 4609, 1988.
24. L. R. Ram-Mohan, S. Saigal, D. Dossa, and J. Shertzer, *Comput. Phys.* **4**: 50, 1990; J. Shertzer, L. R. Ram-Mohan, and D. Dossa, *Phys. Rev. A,* **40**: 4777, 1989.
25. L. R. Ram-Mohan and J. R. Meyer, *J. Nonlinear Opt. Phys. Mat.,* **4**: 191, 1995.

26. C. Parks, A. K. Ramdas, M. R. Melloch, and L. R. Ram-Mohan, *Phys. Rev. B,* **48**: 5413, 1993.
27. L. L. Chang and K. Ploog, (eds.), *Molecular Beam Epitaxy and Heterostructures* Dordrecht: Martinus Nijhoff, 1985; NATO Adv. Sci. Inst. Ser. E87, 1-719, 1985.
28. G. B. Stringfellow, *Organometallic Vapor Phase Epitaxy: Theory and Practice,* Boston: Academic Press, 1989.
29. Y. P. Varshni, *Physica,* **34**: 149, 1967.
30. S. Zollner, S. Gopalan, and M. Cardona, *Solid State Commun.,* **77**: 485, 1991; C. K. Kim, P. Lautenschlager, and M. Cardona, *Solid State Commun.,* **59**: 797, 1986.
31. F. H. Pollak and H. Shen, *Superlattices and Microstructures,* **6**: 203, 1989.
32. A. Kangarlu, H. R. Chandrasekhar, M. Chandrasekhar, Y. M. Kapoor, F. A. Chambers, B. A. Vojak, and J. M. Meese, *Phys. Rev. B,* **37**: 1035, 1988.
33. P. Lautenschlager, M. Garriga, S. Logothetidis, and M. Cardona, *Phys. Rev. B,* **35**: 9174, 1987.
34. A. Jayaraman, Diamond anvil cell and high-pressure physical investigations, *Rev. Mod. Phys.,* **55**: 65–108, 1983.
35. S. Satpathy, M. Chandrasekhar, H. R. Chandrasekhar, and U. Venkateswaran, *Phys. Rev. B,* **44**: 11339, 1991.
36. U. Venkateswaran, M. Chandrasekhar, H. R. Chandrasekhar, T. Wolfram, R. Fischer, W. T. Masselink, and H. Morkoc, *Phys. Rev. B,* **31**: 4106, 1985.
37. U. Venkateswaran, M. Chandrasekhar, H. R. Chandrasekhar, B. A. Vojak, F. Chambers, and J. Meese, *Phys. Rev. B,* **33**: 8416, 1986.
38. A. Kangarlu, H. R. Chandrasekhar, M. Chandrasekhar, Y. M. Kapoor, F. A. Chambers, B. A. Vojak, and J. M. Meese, *Phys. Rev. B,* **38**: 9790, 1988.
39. D. J. Wolford, T. F. Kuech, J. A. Bradley, M. A. Gell, D. Ninno, and M. Jaros, *J. Vac. Sci. Technol.,* **B4**: 1043, 1986.
40. G. Li, D. Jiang, H. Han, Z. Wang, and K. Ploog, *Phys. Rev. B,* **40**: 10430, 1989.
41. M. Holtz, R. Cingolani, K. Reimann, R. Muralidharan, K. Syassen, and K. Ploog, *Phys. Rev. B,* **41**: 3641, 1990; M. Holtz, K. Syassen, R. Muralidharan, and K. Ploog, *Phys. Rev. B,* **41**: 7647, 1990.
42. P. Lefebvre, B. Gil, and H. Mathieu, *Phys. Rev. B,* **35**: 5630, 1987.
43. E. O. Kane, In *Semiconductors and Semimetals,* vol. 1. R. K. Willardson (ed.), New York: Academic Press, 1966.
44. B. Rockwell, H. R. Chandrasekhar, M. Chandrasekhar, F. H. Pollak, H. Shen, L. L. Chang, W. I. Wang, and L. Esaki, *Surface Sci.,* **228**: 322, 1990.
45. S. Zollner, S. Gopalan, and M. Cardona, *Solid State Commun.,* **76**: 877, 1990.
46. M. Chandrasekhar and F. H. Pollak, *Phys. Rev. B,* **15**: 2127, 1977.
47. C. Jagannath, E. S. Koteles, J. Lee, Y. J. Chen, B. S. Elman, and J. Y. Chi, *Phys. Rev. B,* **34**: 7027, 1986.
48. P. Lefebvre, B. Gil, H. Mathieu, and R. Planel, *Phys. Rev. B,* **39**: 5550, 1989; P. Lefebvre, B. Gil, H. Mathieu, and R. Planel, *Phys. Rev. B,* **40**: 7802, 1989.
49. J. Lee, M. O. Vassell, E. S. Koteles, C. Jagannath, K. T. Hsu, G. J. Jan, C. P. Liu, and I. F. Chang, *Phys. Rev. B,* **40**: 1703, 1989.
50. G. Platero and M. Altarelli, *Phys. Rev. B,* **36**: 6591, 1987.
51. W. R. Tribe, P. C. Klipstein, R. Grey, J. S. Roberts, and G. W. Smith, *J. Phys. Chem. Solids,* **56**: 429, 1995.
52. W. R. Tribe, P. C. Klipstein, G. W. Smith, and R. Grey, *Phys. Rev. B,* **54**: 8721, 1996, and the references therein.
53. L. Schultheis, K. Kohler, and C. W. Tu, *Phys. Rev. B,* **36**: 6609, 1987.
54. J. S. Weiner, D. A. B. Miller, D. S. Chemla, T. C. Damen, C. A. Burrus, T. H. Wood, A. C. Gossard, and W. Wiegman, *Appl. Phys. Lett.,* **47**: 1148, 1985.
55. G. Danan, F. R. Ladan, F. Mollot, and R. Planel, *Appl. Phys. Lett.,* **51**: 1605, 1987.
56. M.-H. Meynadier, R. E. Nahory, J. M. Worlock, M. C. Tamargo, J. L. de Miguel, and M. D. Sturge, *Phys. Rev. Lett.,* **60**: 1338, 1988.
57. D. A. B. Miller, D. S. Chemla, and S. Schmitt-Rink, *Phys. Rev. B,* **33**: 6976, 1986.
58. K. Yamanaka, T. Fukunaga, N. Tsukada, K. L. I. Kobayashi, and M. Ishii, *Appl. Phys.Lett.,* **48**: 840, 1986.
59. G. Bastard, J. A. Brum, and R. Ferreira, In *Solid State Physics,* vol. 44, H. Ehrenreich and D. Turnbull (eds.), Boston: Academic Press, 1991, p. 229.
60. P. Bhattacharya, In *Semiconducting Opto-Electronic Devices,* Upper Saddle River, NJ: Prentice Hall, 1997.
61. S. L. Chuang, *Physics of Optoelectronic Devices,* New York: Wiley, 1995.

H. R. Chandrasekhar
Meera Chandrasekhar
University of Missouri-Columbia